Research Article | Vol. 9, No. 3 | 1 Mar 2019 | OPTICAL MATERIALS EXPRESS 976
Optical Materials EXPRESS

Size-dependent off-resonant nonlinear optical properties of gold nanoparticles and demonstration of efficient optical limiting

YUE FU,[1,2] RASHID A. GANEEV,[1,4] P. S. KRISHNENDU,[1] CHUNYANG ZHOU,[1] KONDA SRINIVASA RAO,[1] AND CHUNLEI GUO[1,3,5]

[1] *The Guo China-US Photonics Laboratory, State Key Laboratory of Applied Optics, Changchun Institute of Optics, Fine Mechanics and Physics, Chinese Academy of Sciences, Changchun 130033, China*
[2]*University of Chinese Academy of Sciences, Beijing 100049, China*
[3]*The Institute of Optics, University of Rochester, Rochester, NY 14627, USA*
[4]*rashid@ciomp.ac.cn*
[5]*guo@optics.rochester.edu*

Abstract: There are different possibilities for the applications of gold nanoparticles in various areas of optoelectronics. Here we report the nonlinear optical studies of chemically prepared gold nanoparticle suspensions using femtosecond pulses. The nonlinear refractive indices, nonlinear absorption coefficients, and saturated intensities of the nanoparticles of different sizes are measured at the wavelengths of 400 and 800 nm. We also demonstrate the optical limiting of 800 nm, 60 fs pulses during propagation through these suspensions. The competition of saturable and reverse saturable absorption in the case of 400 nm radiation is analyzed. The intensity-dependent transformation from saturable absorption to reverse saturable absorption indicates that these gold nanoparticles can be useful for eye protection, pulse shaping and passive mode locking.

1. Introduction

Gold nanoparticles (GN) have been extensively studied due to possibilities for their use in different areas of nonlinear optics, optoelectronics, and laser physics. The applications of GN include optical limiting, optical switching, plasmonic waveguides, photovoltaics, catalysis, drug delivery in medical science, nanotechnologies, spectroscopy and spectrophotometry, electrochemical and bioelectrochemical analysis, etc [1–6]. Their unique optoelectronic properties are related with the surface plasmons at around λ = 530 nm, which being excited in the vicinity of this wavelength cause the enhancement of optical and nonlinear optical response. Meanwhile, for the infrared and blue excitation wavelengths (800 and 400 nm corresponding to the Ti: Sapphire laser radiation and its second harmonic respectively), which emit out from the surface plasmon resonance (SPR) of GN, other factors like intraband transitions should also be taken into account. The SPR and thereby the optical response of GN can be tuned by varying the size or shape of the nanoparticles leading to necessity in their analysis to define the customized optical properties for different applications.

GN in the form of colloidal solutions were previously prepared using either chemical or laser ablation methods. The difference between these methods consists in different size characteristics of the nanoparticles produced. In previous studies, a dynamics of the spatial and nonlinear optical parameters of GN was noted, but the mechanisms responsible for these variations have not been clarified to a sufficient extent. Optical nonlinearities of GN were the subject of a number of studies during the past two decades. In particular, it has been shown that the nonlinear refractive index of the gold colloidal solution has a considerable value [7]. Those studies of gold aggregates at the wavelength of 532 nm, i.e. at resonance conditions

#349935 https://doi.org/10.1364/OME.9.000976
Journal © 2019 Received 2 Nov 2018; revised 15 Dec 2018; accepted 19 Dec 2018; published 4 Feb 2019

Optical Materials EXPRESS

with the SPR band of GN, have shown that the changes of the refraction index can be due to different physical mechanisms.

Saturable absorption (SA) and reverse saturable absorption (RSA) using the 532 nm excitation are two familiar nonlinear absorption types in metal nanoparticles [8]. SA and RSA are related to the decreasing and increasing in the absorption, respectively. For GN, the SA effect at resonance conditions (i.e. close to λ = 530 nm) can mainly be attributed to the ground-state plasmon bleaching of the intraband transition in the *s-p* conduction band at moderate pump intensities. As the SA bands belong to the visible range, the GN possess the potential of Q-switchers for short pulses generation in this region [9]. Additionally, the RSA effect can be related with the free-carrier absorption or two-photon absorption (2PA). The changes from a negative value of nonlinear absorption to a positive one with increasing pulse energy suggest that the primary nonlinear absorption in GN has been transformed from SA to RSA process, which can be useful for optical limiting of propagating radiation.

Optical limiting (OL) is one of potential applications of the materials' optical nonlinearities. It aimed in protecting eyes and sensitive registration devices from damaging. Previously, small-sized species, like nanoparticles and quantum dots, have shown the advantages in their use for OL [10,11]. The mechanisms that cause OL have different origins. RSA, which takes place due to enhanced absorption from excited states, is responsible for OL in colloidal metal compounds [12,13] and fullerenes [14]. 2PA is responsible for OL in semiconductor structures [15]. Excited state induced process is one of the main sources of optical nonlinearities, which has potential applications for OL [16]. Thus a search of enhanced population of these states in the case of various nanoparticle solutions is worth to continue by using the size-related variations of their nonlinear optical response at off-resonant conditions. Additionally, a search of effective optical limiters at 800 nm is useful for practical applications.

The enhanced nonlinear optical properties of nanoparticles as compared to those of the bulk state make nanoscale particles more promising for designing optoelectronic and micro-electronic devices. In this connection, the growing interest in GN is related to their unique optical, morphological, and electronic properties that are based on the quantum-confinement effect [17]. Many types of studies for GN with different shapes (sphere, cube, octahedron, rod, etc.) have been carried out [18–23]. The theoretical models have brought forward an understanding of the origin of these fascinating phenomena in GN [24].

Above analysis shows that the optical nonlinearities of GN under 530 nm resonant conditions has been studied extensively. Meanwhile, the analysis of the off-resonant nonlinear optical behavior of synthesized GN of different sizes at around 800 and 400 nm or even shorter wavelengths is of special importance. Some variations of the third-order nonlinear properties in GN have been found for wavelengths at around 800 nm [24]. Meanwhile, the role of spatial characteristics of nanoparticles at off-resonant conditions yet took attention during previous studies of GN. The size dependent variations of nonlinear optical characteristics along with the strong nonlinear optical absorption of both large (>50 nm) and small (<20 nm) GN under 400 and 800 nm femtosecond pulses can be used for different applications, such as high-order harmonic generation in "optimally" prepared GN plasmas, optical limiting and switching, etc.

In this paper, we present the results of studying the optical, structural, and nonlinear optical characteristics of the GN suspensions prepared using the chemical technique. A systematic study of the third-order optical nonlinearities of the GN of four different sizes is discussed. We analyze the variable nonlinear optical response of these nanoparticles. We also present the optical limiting studies in GN suspension.

Optical Materials EXPRESS

2. Experimental methods

2.1. Synthesis of GN suspensions

Gold nanoparticles can be synthesized by different methods. Since the optical, and especially nonlinear optical, properties are strongly governed by GN sizes, morphology, and surrounding environment, we chose a modified preparation of the Turkevich citrate method [25] for the synthesis of four different sizes of nanoparticles. The sizes of the GN were controlled by quantitatively varying the addition of the trisodium citrate (stabilising and reducing agent) to tetrachloroauric acid.

GN were prepared by the reduction of tetrachloroauric acid ($HAuCl_4$) with trisodium citrate ($Na_3C_6H_5O_7$). The $HAuCl_4$ solution (1% 2 mL) and deionised water (48 mL) were heated until boiling. Then specific quantities of trisodium citrate along with deionized water (5 mL) were added quickly into this boiling mixture under vigorous stirring. The solution turned from yellow to wine-red color and then the heating was stopped after 15 minutes. The stirring was continued for 30 more minutes until the reaction mixture was cooled down. To prepare the GN suspensions of different sizes, 0.0143, 0.0285, 0.114 and 0.228 g of trisodium citrate were added during the process to stabilize and reduce the $HAuCl_4$ and to obtain a descending size distribution of GN. The particle size and the shape of prepared samples were determined using a scanning electron microscope (SEM, S-4800, Hitachi) and a transmission electron microscope (TEM, JEM 2100F, JEOL).

2.2. Optical and nonlinear optical measurements

The absorption measurements of samples were performed using a UV-Vis spectrophotometer (Cary Series, Agilent Technologies). The optical spectra were measured in the range of 400 to 800 nm to detect the characteristic SPR and visible light absorption of GN suspensions.

The conventional Z-scan scheme was used to study the off-resonant third-order nonlinear optical properties of GN suspensions (Fig. 1). The 800 nm, 60 fs pulses from Ti: Sapphire laser (Spitfire Ace, Spectra-Physics) operated at 1 kHz repetition rate were focused using the 400 mm focal length spherical lens along the Z axis through which the GN suspension filled in a 2 mm thick silica glass cell was displaced. To generate the second harmonic pulses (λ = 400 nm), a BBO crystal was used. The 200 ps pulses were also available from this laser by extracting part of uncompressed radiation. The spatial distribution of focused beam was found to be close to the Gaussian shape with the 42 and 76 μm full widths at half maximum and $1/e^2$ maximum of intensity distributions respectively, which was defined using a CCD camera (Thorlabs). The variations in the normalized transmittances of samples in the closed-aperture (CA) and open-aperture (OA) Z-scan schemes were measured using a fast photodetector. An aperture sizes of CA scheme (1.5 mm) allowed transmittance of ~10% of the radiation propagated through the samples.

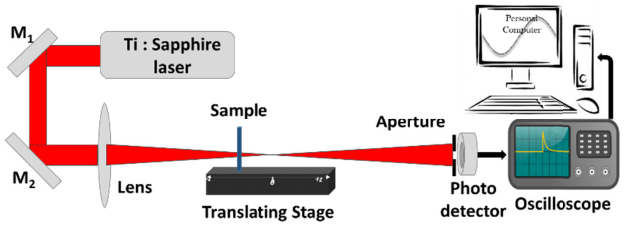

Fig. 1. Experimental setup for Z-scan measurements.

Our Z-scan scheme was calibrated using a 1-mm-thick fused silica plate. The calculations using the fitting procedure allowed definition of the nonlinear refractive index of this material at 800 nm to be (3.0 ± 0.7) × 10^{-16} cm^2 W^{-1}. This value is close to earlier reported measurements of the γ of fused silica at this wavelength (3 × 10^{-16} cm^2 W^{-1} [26], (2.7 ± 0.3) ×

Optical Materials EXPRESS

10^{-16} cm^2 W^{-1} [27]). The error bars (± 5%) of these measurements were the same during the entire course of the experiments. The error bars of definition of the absolute values of γ and β were estimated to be ± 25% due to uncertainty in the measurements of the intensity of laser pulses in the focal plane.

The OA and CA Z-scans were fitted using standard equations of Z-scan theory. The normalized transmittance in the case of 2PA and SA for OA Z-scan measurements is given by the equations:

$$T_{2PA} \approx 1 - \frac{q}{2\sqrt{2}} \tag{1}$$

$$T_{SA}(z) = 1 + \frac{I_0}{I_{sat}}\left(1 + \frac{z^2}{z_0^2}\right)^{-1} \tag{2}$$

Here, $q = \beta I_0 L_{eff}/(1 + z^2/z_0^2)$, where β is the nonlinear absorption coefficient, $z_0 = k(w_0)^2/2$ is the Rayleigh length, $k = 2\pi/\lambda$ is the wave number, w_0 is the beam waist radius at the $1/e^2$ maximum of intensity distribution, $L_{eff} = [1\text{-}\exp(-\alpha_0 L)]/\ \alpha_0$ is the effective length of the medium, α_0 is the linear absorption coefficient, L is the sample thickness, I_0 is the intensity of incident beam at the focal area and I_{sat} is the saturation intensity which is related to the concentration of the sample and corresponds to the case when transmittance through the sample increases twice due to bleaching process.

The normalized transmittance in the case of nonlinear refraction and absorption (NRA) along with the combination of nonlinear refraction (NR) and SA for the CA Z-scan is given by the equations:

$$T_{NRA}(z) = 1 + \frac{2(-\rho x^2 + 2x - 3\rho)}{(x^2+1)(x^2+9)}\Delta\phi_0 \tag{3}$$

$$T_{NRA+SA}(z) = 1 + \frac{4x}{(x^2+1)(x^2+9)}\Delta\phi_0 + \frac{I_0}{I_{sat}(x^2+1)} \tag{4}$$

Here $\rho = \beta/2k\gamma$, γ is the nonlinear refractive index, $x = z/z_0$ and $\Delta\Phi_0 = k\gamma I_0 L_{eff}$ is a phase change due to nonlinear refraction. The corresponding β and γ are calculated from the fitting equations to determine the nonlinear absorption and refraction of GN suspensions respectively.

3. Morphological and optical analysis of GN suspensions

The particle size distribution and the morphology of synthesized GN were determined from the SEM and TEM images [Fig. 2(a)]. The mean diameters of GN were found to be 64, 32, 17, and 13 nm in the case of addition of different amount of trisodium citrate to the mixture. It was distinctly observed that the increase of trisodium citrate led to a decrease of GN sizes, which has shown that the relative concentration of the precursor and the reducing agent strongly affect the nucleation and the growth progression of GN. For particles below 20 nm, the size distribution was comparatively homogeneous and the standard deviation from mean size was minimum. Electron microscopy of suspensions [Fig. 2(b)] demonstrated no changes in the size parameters of the nanoparticles occurring during two months period. The size distribution of GN remained stable as well.

Optical Materials EXPRESS

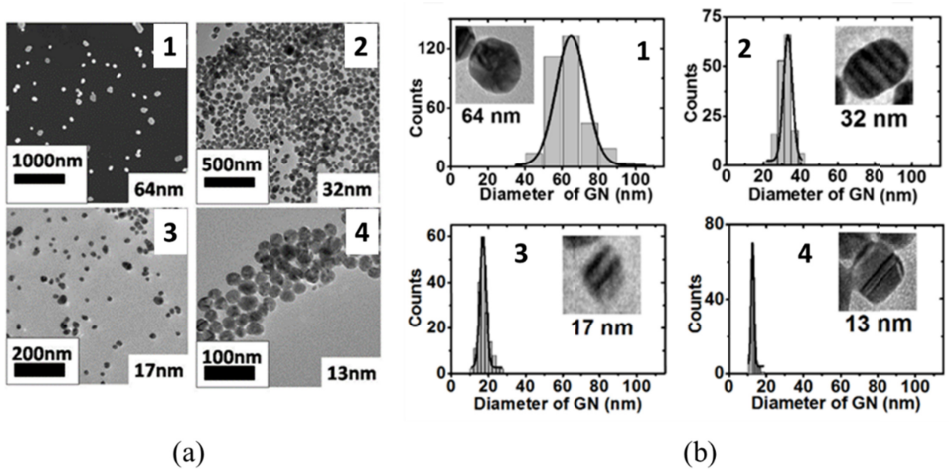

Fig. 2. (a) SEM image of (1) 64 nm GN. TEM images of (2) 32, (3) 17, and (4) 13 nm GN. (b) Histograms of corresponding nanoparticles and images of single GN.

The optical properties of GN show the characteristic absorption dominated by SPR peaks at 537, 528, 526, and 521 nm for particle sizes of 64, 32, 17, and 13 nm respectively [Fig. 3]. For the metal nanoparticles, the size controllability and surface tenability are essential. The electronic and optical properties exploited in their applications are highly dependent on the particle size and shape. The red shift is also accompanied by a broadening of the SPR band. The red shift increased with the increase in particle size and is characterized by appearance of blue colored solution. The absorption spectrum is determined by the localized surface plasmon resonance of the metal nanoparticles in the suspension [28].The broad range of particle sizes and shape distributions for 64 nm GN resulted in a notably broader absorption spectrum. The width and position of SPR was varied as a function of particle size and shape (see inset in Fig. 3).

As has been previously pointed out in a number of studies, the absorption spectra of GN can be controlled, to a considerable extent, by the parameters and methods of preparation of the nanoparticle-contained solutions. The positions of the SPR of these colloidal suspensions prepared by chemical methods correspond to the range of 530 - 550 nm, whereas, in the case of laser ablation, the peak of the SPR is slightly shifted toward shorter wavelengths due to the influence of small-sized particles. Variations of the absorption spectra of the chemically prepared GN were analyzed during two months and no significant changes were observed.

Previously, the aggregation and precipitation of GN were the main reasons for variation of the optical and nonlinear optical properties of the nanoparticle suspensions obtained by chemical and laser ablation methods. Note that the nonlinear optical studies described in this paper were performed at the conditions of the stabilization of the size and spectral characteristics of the GN in the suspensions. The studies were carried out in the spectral regions corresponding to single (in the case of 400 nm radiation) and two-photon (in the case of 800 nm radiation) absorption in the suspensions containing GN. These nanoparticles showed mostly spherical shape. Notice that the absorption peak at around 527 nm corresponds to a commonly reported SPR of the spherical GN.

Optical Materials EXPRESS

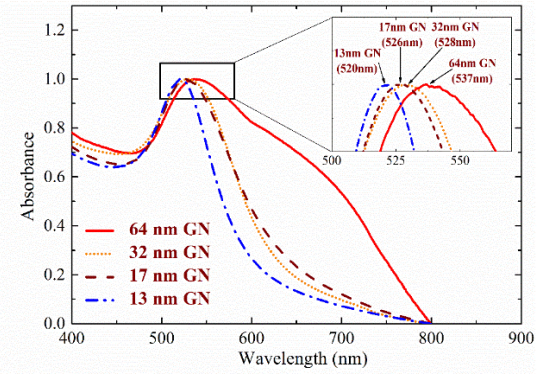

Fig. 3. Absorption spectra of different GN. Inset shows the enlarged area of the maximums of the SPR of different GN.

Once the sizes of nanoparticles increase, their peak of plasmon resonance will be tuned towards longer wavelength and vice versa. One can use Mie and Drude theory to show that the sizes of GN can be calculated from their absorption spectra. The bandwidth of SPR has earlier been used [29] to estimate GN sizes according to the equation

$$\Delta\omega_{1/2} = \nu_F / R \tag{5}$$

where $\Delta\omega_{1/2}$ is the half width of the absorption band, R is the GN radius in nanometers, and F is the Fermi velocity of conduction electrons in gold (1.39×10^{15} nm/s). By applying this formula, which is useful for small particles (R < 20 nm), we estimated the diameter of GN in our suspension (11 nm). This value is close to the direct measurements of the mean size of GN using the TEM images (13 nm).

4. Nonlinear optical studies

4.1. OA Z-scans

The main nonlinear optical process observed using OA scheme at λ = 800 nm and related to the small-sized GN was the nonlinear absorption [Fig. 4(a)]. This process has earlier been associated with the RSA [30]. These OA Z-scans were obtained in the case of the suspensions containing 13, 17, and 32 nm nanoparticles. The values of the nonlinear absorption coefficients for these three GN suspensions were calculated to be 1.5×10^{-12}, 1.5×10^{-12}, and 2×10^{-12} cm W^{-1} respectively. These data were defined by the fitting procedure using Eq. (1). We also observed a nonlinear absorption in these suspensions in the case of 400 nm pulses. In this case the process was also attributed to RSA [Fig. 4(b)]. The measured values of the nonlinear absorption coefficients attributed to RSA in these three GN suspensions were 1×10^{-11}, 1.5×10^{-11}, and 1.2×10^{-11} cm W^{-1} respectively, which are larger than in the case of longer wavelength pulses. No effect of the fused silica cell and water was observed up to $I_0 = 3 \times 10^{11}$ W cm^{-2}.

In the meantime, the SA was observed in the case of the suspension containing 64 nm GN by using both 800 and 400 nm pulses. Though the SA in the case of 800 nm pulses was relatively weak [$|\Delta T| \leq 0.075$, Fig. 4(a), upper curve], its influence was notably increased in the case of shorter wavelength (400 nm) pulses [$|\Delta T| \sim 0.2$, Fig. 4(b), upper curve] even at significantly smaller intensity. This wavelength-dependent growth of SA is a commonly observed feature attributed to larger cross section of population of the excited states responsible for RSA in the case of shorter wavelength excitation.

The electric field polarizing a nanoparticle may substantially exceed the external applied field. The most remarkable manifestation of this effect is related to the plasmonic properties, which enhance the nonlinear optical characteristics of the medium in the vicinity of the

Optical Materials EXPRESS

central wavelength of SPR, especially in the case of resonant excitation. This resonance can be considered in the framework of the model of collective oscillations of surface electrons in a nanoparticle. However, in our case (800 and 400 nm pulses) the excitation occurs far from the SPR band of GN (~530 nm). Thus the SA of our GN hardly could be attributed only to the influence of SPR, which is the coherent coupling between free electrons of the conduction band and the external electromagnetic field emitting at approximately similar wavelength [31].

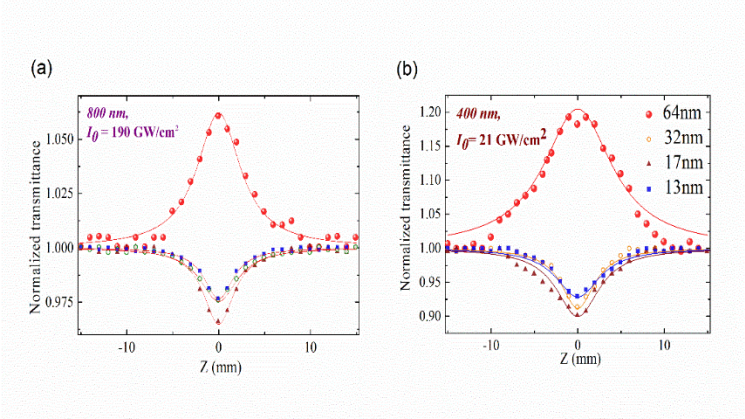

Fig. 4. OA Z-scans of suspensions containing different GN using (a) 800 and (b) 400 nm, 40 fs pulses at the intensities of 1.9×10^{11} and 4.5×10^{10} W cm^{-2} in the focal plane.

Variation of 400 nm pulse energy strongly affected the Z-scan of the suspension containing 64 nm GN and changed the role of SA. In Fig. 5, we present the dependence of normalized transmittance on the position of the suspension containing 64 nm GN at different energies of 400 nm pulses. The absorption spectrum of this solution shows broad linear absorption band centered at the wavelength of ~530 nm (Fig. 3, solid line). SA was steadily overpassed by RSA with the growth of pulse energy from 38 to 410 nJ. Standard OA Z-scan fitting allowed determining sign and magnitude of positive and negative nonlinear absorption coefficients, as well as saturation intensity of this suspension.

One can see that SA, which dominates over RSA at relatively small energies of 400 nm pulses [E = 38 nJ, empty circles in Fig. 5(a)], becomes less pronounced at higher pulse energies (E > 130 nJ, see other curves) with regard to the growing RSA effect. This difference in the involvement of SA and RSA is clearly seen in the area close to the focal plane of focusing lens (i.e. near z = 0 mm where laser radiation had largest intensity). The gradual growth of pulse energy led to appearance of deeper valley and larger decrease of normalized transmittance in the vicinity of z = 0 mm [down to $T \approx 0.6$; E = 318 nJ, filled triangles in Fig. 5(c)]. Finally, at E = 410 nJ, only RSA was dominated over all range of normalized transmittance variations [empty triangles, Fig. 5(d)]. The intensity of laser pulses at these conditions was close to the one at which largest value of optical limiting can be achieved at λ = 400 nm (5×10^{11} W cm^{-2}; see also subsection 4.2).

The nonlinear absorption coefficients at λ = 400 nm in the cases including SA and RSA were analyzed by the $\alpha(I) = \alpha_0 \times I/(1 + I/I_{sat}) + \beta \times I = \alpha_{SA} + \alpha_{RSA}$ relation for intensity-dependent absorption coefficient [19]. Here I is the intensity of laser pulse. This absorption coefficient consisted on two parts: one related with saturable absorption (α_{SA}) and another related with reverse saturable absorption (α_{RSA}). Using this model we found the saturation intensity ($I_{sat} = 4 \times 10^{11}$ W cm^{-2}) for used GN suspension. The β of this 64 nm GN suspension associated with RSA [Fig. 5(d)] was calculated to be 7×10^{-10} cm W^{-1} (at λ = 400 nm). One can estimate the β of nanoparticles to be 7×10^{-6} cm W^{-1} taking into account the volume part

Optical Materials EXPRESS

of 64 nm GN in the solution (10^{-4}). This strong RSA-associated nonlinear absorption was responsible for the optical limiting of 400 nm radiation.

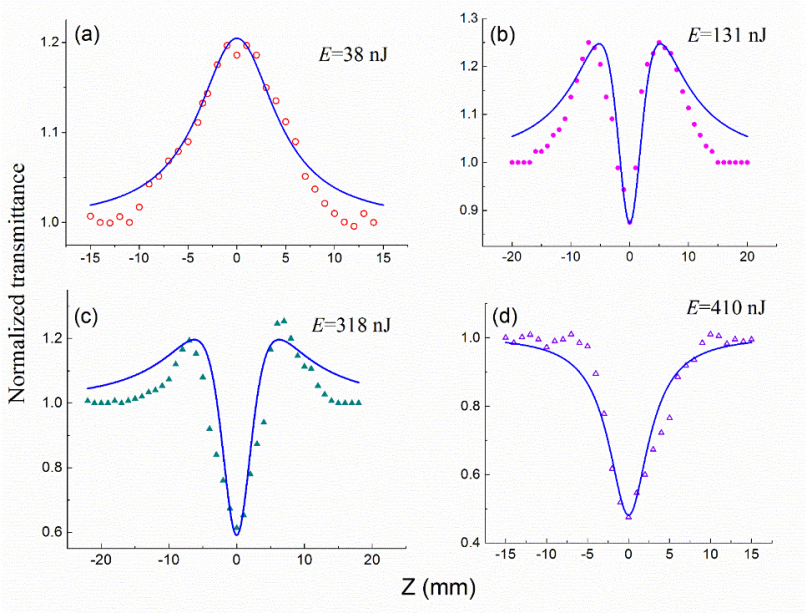

Fig. 5. OA Z-scans of the suspension containing 64 nm GN using 400 nm pulses of different energy. [(a) 38, (b) 131, (c) 318 and (d) 410 nJ]. Solid curves [(a) and (d)] are fitted with experimental data in accordance with the relations of phenomenological model of SA and Z-scan theory.

A five-level model is used to interpret the RSA process [32]. Such absorption in the medium requires the fulfillment of the following basic criteria: firstly, the material must have an excited-state absorption cross-section larger than the ground-state absorption cross-section, and secondly, the lifetime of the excited state must be long enough [in comparison with the pulse duration (t) of the laser radiation]. Each of studied GN satisfy these criteria, which allow observation of such variations of normalized transmittance (T) of the GN suspensions, allowing an entire suppression of SA at the used conditions of experiments (λ = 400 nm, t = 60 fs, $E \approx 0.4$ μJ).

Below we discuss the observation of different nonlinear absorption processes at 800 and 400 nm [Figs. 4 and 5]. One can see that, depending on particles sizes, the nonlinear absorption shows different sign (Fig. 4). SA was observed for larger sized nanoparticles, while smaller sized nanoparticles demonstrated TPA (in the case of 800 nm radiation) and RSA (in the case of 400 nm radiation). SA has been observed previously in various media (glasses doped with semiconductor nanoparticles, dyes, thin polythiophene films, etc.) in the IR, visible, and UV ranges. We analyzed this process at two wavelengths (800 and 400 nm) in the case of the suspension containing 64 nm nanoparticles. The dependence of the normalized transmittance in that case may be represented in the form of Eq. (2) or Eq. (1) with a negative β. The parameter β in that case can be represented by the ratio of the linear absorbance to the saturation intensity ($\beta = -\alpha/I_{sat}$). The theoretical dependence for 64 nm GN presented in Fig. 5(a) allowed defining $\beta = -4 \times 10^{-11}$ cm W^{-1}.

Earlier, a saturable absorption in this medium was reported in the case of 532 nm laser pulses [33]. A weak negative refraction and a nonlinear absorption in GN using 792 nm radiation were demonstrated as well. Previous studies reported the values of saturated intensity and negative nonlinear absorption coefficient of GN suspensions (9×10^{9} W cm^{-2} and -8×10^{-11} cm W^{-1} respectively) [33]. The appearance of SA in those studies was

Optical Materials EXPRESS

attributed to bleaching of the ground state at moderate intensities. Notice that the signs of nonlinear refractive indices and nonlinear absorption coefficients of GN were reported to be either negative or positive. Probably, this discrepancy can be attributed to the difference in the involvement of the local field of nanoparticles on the variation of the magnitude and sign of β and γ.

4.2. Optical limiting

OL materials based on noble metal nanoparticles are attractive, because gold and silver nanoparticles are easy to prepare, and they are highly soluble and stable in aqueous and organic solvents. The optical, nonlinear optical and optical limiting properties of gold and silver nanoparticles strongly depend on their size, shape, surrounding matrix, and solvent in which the nanoparticles are dissolved. Previously, considerable efforts have been focused on investigating the relationships between the OL and nonlinear optical properties of GN and their size and shape (nanostars, nanospheres, nanorods, nanoshells, bipyramidal, etc). In the case of nanosecond pulses, the GN exhibited intensity-dependent transformation from SA to RSA. Thus, the GN were found to display strong OL properties in the case of relatively long and high energy laser pulses [34]. The improved OL response in GN has earlier been discussed from the viewpoint of structural characteristics.

In our studies, the OL was demonstrated using the 800 nm, 60 fs pulses propagating through the suspension containing 17 nm GN in water. This effect is attributed to RSA. The suspension was placed close to the focal plane of 400 mm focal length lens. We gradually increased the energy of 800 nm pulses and measured the output radiation propagated through the 2-mm-thick cell containing GN suspension [Fig. 6(a)]. The linear dependence between input and output pulses was maintained up to the input pulse energy of ~0.11 μJ [Fig. 6(b), filled spheres]. Further grow of input pulse energy led to OL of the energy of propagated laser radiation.

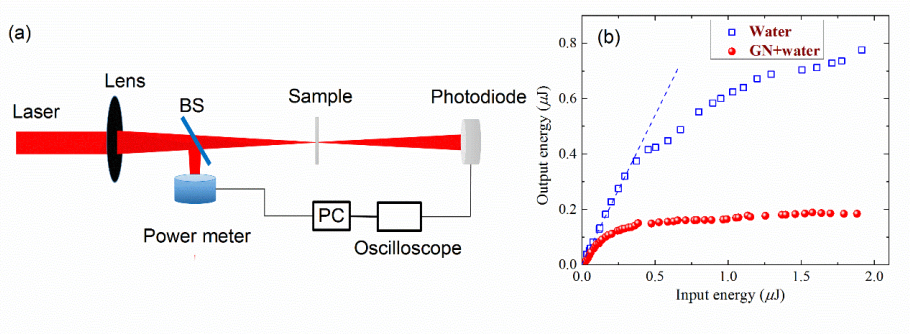

Fig. 6. (a) Setup for optical limiting studies. (b) Optical limiting of 800, 60 fs pulses in water and suspension containing 17 nm GN.

The energy of propagated pulse was stabilized at ~0.15 – 0.17 μJ. This process was maintained up to the input energy of 2 μJ above which stronger impeding processes worsened the propagation of laser pulses. Similar study in pure water showed no declination from the linear dependence up to E_{output} ≈0.35 μJ of output radiation [Fig. 6(b), empty circles]. At these conditions the coefficient of optical limiting induced suppression of propagating radiation in GN suspension compared to pure water was measured to be ~2.5. Further growth of input energy (i.e. above E_{input} = 0.4 μJ) led to the growing influence of white light generation in water and declination of E_{input}/E_{output} ratio from the linear dependence. Nevertheless, at highest used input energy (E_{input} ≈1.9 μJ) we achieved the ~4-fold suppression of output pulses in GN suspension compared to the pure water.

Optical Materials EXPRESS

4.3. CA Z-scans

The nonlinear refractive index of metal nanoparticles in different matrices may vary in a wide range, and even change the sign, depending on the conditions of interaction, in particular, in resonant or nonresonant conditions. Under near-resonant conditions, the sign of nonlinear refractive index is determined by the ratio of the fundamental (or double) frequency of laser light and the SPR frequency of the nanoparticles. Our conditions of experiments corresponded to the nonresonant case. Even at these conditions the sign of nonlinear refraction depends on the peculiarities of experiment. Particularly, overheating of our samples by relatively strong 200 ps pulses led to negative nonlinear refraction of 800 nm, 1 kHz pulses, while weaker 60 fs pulses caused positive nonlinear refraction.

Figure 7 shows CA Z-scans of the suspension containing 32 nm nanoparticles using different energies of 200 ps, 800 nm pulses. These Z-scans exhibit different asymmetric peaks followed by valley, which is a typical pattern for the thermal lens induced negative nonlinear refraction attributed to heat accumulation in the area of beam propagation. Similar Z-scans were observed in the case of other small-sized GN suspensions. This asymmetric pattern together with the fact that the laser pulses strongly heat the suspension at 1 kHz repetition rate point out that the origin of observed nonlinear refractive index is related with the thermal process. The pure water did not show such Z-scans even at significantly larger energies of laser pulses. Similar pattern has earlier been reported in Ag_2S suspension [35] and GN colloids [36] using CW radiation of 532 nm pulses.

In our case, the laser pulse interacts with the medium affected by the heating induced by the preceding pulse. The heat accumulation is due to 2PA or RSA and low thermal conductivity of medium. Laser-induced thermal lens effect occurs as energy absorbs from a laser beam, and it turns the medium into a lens for the same beam. The change of refractive index with temperature is caused by a decrease in medium density with increasing temperature [37]. The refractive index will be changed with the change of the thermal lens effect in GN-containing medium by varying the pulse energy. The characteristic time scale for heat dissipation is proportional to R^2 (R is the radius of nanoparticles) The characteristic time constant for heat dissipation depends on the surface area of the particle in accordance with relation τ (ps) = 0.64 × R^2 for R in nanometers [38]. The estimates show that time necessary for the heat dissipation over the focused beam cross section is ~1 ns, and, hence, it is important to take the heat accumulation into account when using radiation with the pulse repetition rate of 1 kHz at relatively high pulse energy.

To confirm the decisive role of the nonlinear absorption in the occurrence of the thermal effect one can note that the distance between peak and valley (ΔZ_{p-v}), i.e. between the maximum and the minimum in the Z-scans, was close to 5 mm, which is equal to $1.2z_0$ (Fig. 7) since Rayleigh length for our focused beam was measured to be ≈4.2 mm. A relation $\Delta Z_{p-v} \approx 1.2z_0$ for Z-scan dependences in the case of the thermal effect caused by the nonlinear absorption is a sign of fifth-order process [33], contrary to the case of third-order nonlinear refraction. In other words, firstly, nonlinear process (either 2PA or RSA) causes the absorption, which further influences the nonlinear refractive properties of medium at relatively high pulse energies.

Optical Materials EXPRESS

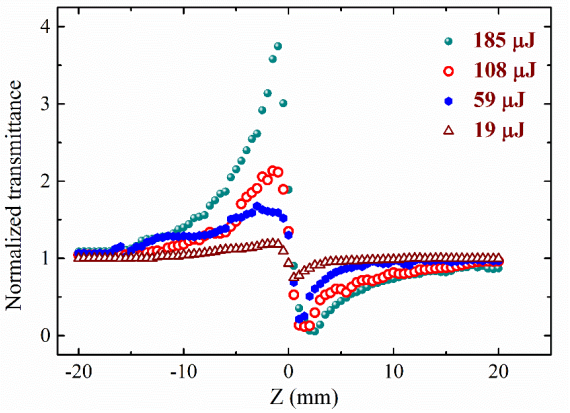

Fig. 7. CA Z-scans of GN suspension using 800 nm, 1 kHz, 200 ps pulses of different energy.

Our investigations of the dependence of ΔT_{p-v} on the pulse energy confirmed the decisive role of the 2PA-induced nonlinear absorption on the whole pattern of Z-scans in the case of small-sized GN. The thermal-induced nonlinear refractive index of GN suspension was calculated to be $\gamma_T = -2 \times 10^{-9}$ cm^2 W^{-1} using the approach developed for nanoparticles dissolved in the water possessing relatively high thermal conductivity (0.6 WmK^{-1}) [39]. One can anticipate the growth of γ_T in the case of other liquids possessing lower thermal conductivity.

Among different processes (intramolecular interaction, orientational Kerr effect, and electronic Kerr effect) contributing to the nonlinear refraction in the case of short laser pulses, the latter effect seems to be the determining one, especially in the case of femtosecond probe pulses. However, as it was shown in Fig. 7, under certain experimental conditions (relatively high pulse energy, longer pulse duration, higher pulse repetition rate, etc.), a considerable contribution to the nonlinear refraction can be also related with the thermal lens effect [37]. This effect can be caused by two processes. The first process is associated with the propagation of an acoustic wave arising due to the absorption of radiation in the medium. As our studies showed, this process is an unimportant component, which do not influence the whole nonlinear refractive pattern of the studied samples. The second process consists of a change in the medium density caused by the accumulation of thermal energy in the absorbing region [38]. It occurs in the case of a low thermal conductivity of the medium and/or a high repetition rate of laser pulses. This process was responsible for observed negative nonlinear refraction in our studies. We also performed similar experiments using same energies at 10 Hz pulse repetition rate and did not observe the thermal lens effect. Indeed, our estimates showed that the relatively small temperature fluctuations do not obviously influence the refractive nonlinearities of the GN suspension.

Optical Materials EXPRESS

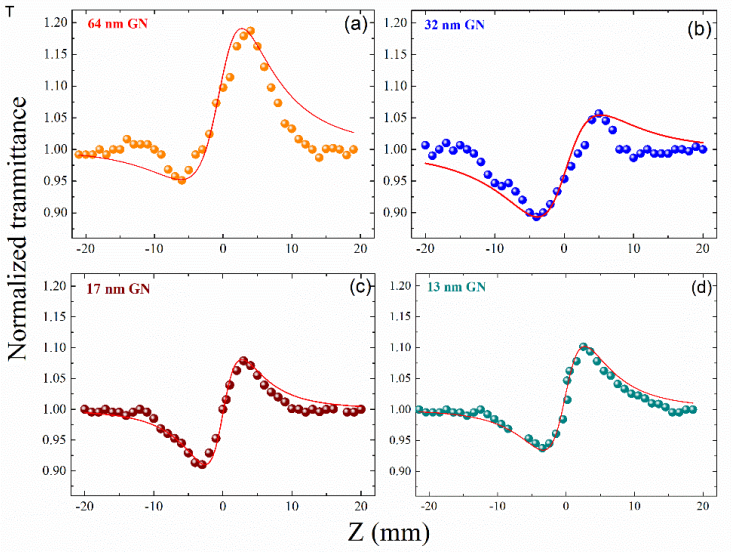

Fig. 8. CA Z-scans of the nanoparticle suspensions containing (a) 64, (b) 32, (c) 17 and (d) 13 nm GN using 800 nm radiation. The energy of 800 nm, 60 fs pulses was 160 nJ. Fitting curves were calculated using Eqs. (3) and (4).

In the case of small energies of laser pulses, no accumulative effects occur at 1 kHz repetition rate. Below we present the CA Z-scans of four GN suspensions containing nanoparticles of different sizes using 800 nm, 160 nJ, 1 kHz, 60 fs pulses (Fig. 8). One can see that all suspensions showed the positive nonlinear refraction characterized by valley followed with peak in the Z-scan pattern. Both SA [Fig. 8(a)] and RSA [Fig. 8(b)] also influence these comparative CA Z-scans, which was manifested by either larger peak or deeper valley. Similar measurements using significantly weaker 400 nm pulses (38 nJ, 1 kHz, 60 fs, Fig. 9) also showed positive nonlinear refraction, with negative and positive nonlinear absorption influencing the whole pattern of CA Z-scans in the cases of the suspensions containing 64, 32 and 17 nm GN [Figs. 9(a)–9(c)]. The use of smaller pulse repetition rate at these experimental conditions resulted in similar results.

From Fig. 8, one can find that the distance between valley and peak (ΔZ_{v-p}), i.e. between the minimum and the maximum in the Z-scans, was about 7.3 mm, which is close to $1.7z_0$. This relation ($\Delta Z_{v-p} \approx 1.7z_0$) for *Z*-scan dependences is a sign of third-order process [39]. The third-order nonlinear response of the studied suspensions mainly originates from pure electronic effects in nanoparticles. These electronic contributions are due to both intraband and interband transitions of gold. The first one corresponds to transitions within the conduction band and the second one corresponds to transitions from the upper levels of the filled *d* band to the levels above the Fermi level in the conduction band.

Optical Materials EXPRESS

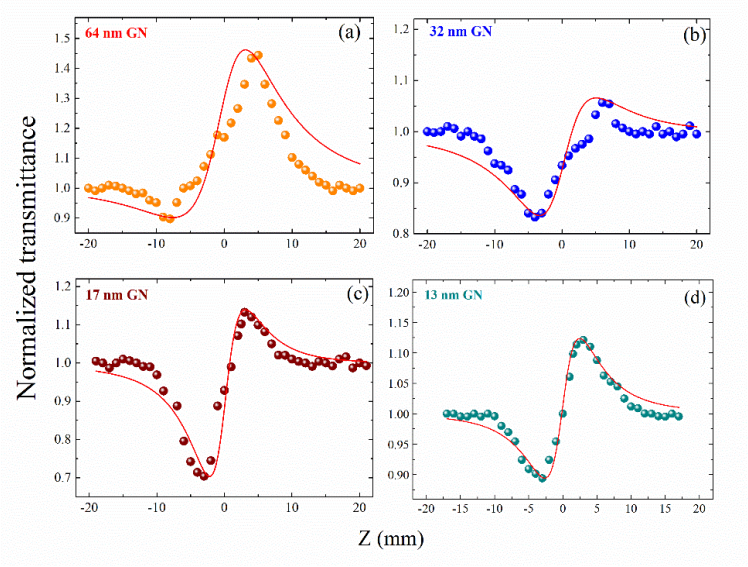

Fig. 9. CA Z-scans of the nanoparticle suspensions containing (a) 64, (b) 32, (c) 17 and (d) 13 nm GN using 400 nm radiation. The energy of 400 nm, 60 fs pulses was 38 nJ. Fitting curves were calculated using Eqs. (3) and (4).

Table 1. Calculated nonlinear optical characteristics of four GNs.

NLO measurements of Au NPs				
	λ = 800 nm, t = 60fs, 1kHz, E = 160 nJ		λ = 400 nm, t = 60fs, 1kHz, E = 38 nJ	
Diameter	γ (cm^2/W) (× 10^{-10})	β (cm/W) (× 10^{-7}) OA	γ (cm^2/W) (× 10^{-10})	β (cm/W) (× 10^{-7}) OA
64 nm	0.18	–0.7 (I_{sat} = 5.7 × 10^{-12} W/cm^2)	–2.3	–2.7 (I_{sat} = 4 × 10^{-11} W/cm^2)
32 nm	0.13	0.84	1	9
17 nm	0.14	0.59	2	7.2
13 nm	0.13	0.56	1.1	5.8

Previously, influence of GN sizes on the third-order nonlinearity of PVA films was reported in Ref [40]. Three samples of GN with different sizes were produced by laser ablation method. They were used to produce GN doped PVA thin films. Using Z-scan technique, the nonlinear refractive index and nonlinear absorption coefficient of films were measured under the irradiation of the second harmonic of a low power CW Nd:YAG laser. Results show that by decreasing the size of nanoparticles in the range of 9–20 nm, the nonlinear refractive index of Au doped PVA films decreases while their nonlinear absorption coefficient increases. Thermo-optical coefficient of samples was also calculated. Increasing the size of nanoparticles led to increase of their thermo-optical coefficient.

Optical Materials EXPRESS

The calculations of nonlinear refractive indices of our GN suspensions were carried out using the standard fitting procedure (Eq. (3). The γ at two wavelengths were calculated to be $\gamma_{800\ nm} = 1.4 \times 10^{-11}$ cm^2 W^{-1} and $\gamma_{400\ nm} = 2 \times 10^{-10}$ cm^2 W^{-1} (both for 17 nm GN suspension). The thermal-induced variation of nonlinear refraction in these conditions is minimal, contrary to the case shown in Fig. 7. Notice that thermal-induced processes may play important role in the case of high pulse repetition rate (MHz [41],), as well. The calculated data of the nonlinear optical characteristics of different GNs are collected in Table 1.

The variable strong nonlinear optical response of chemically prepared nanoparticles will allow further use of these properties in manipulating micro- and nanoparticles by optical nonlinear endoscopy [42], analysis of localized plasmon modes in disordered nanoantennas [43], direct imaging of the near field and dynamics of SRP on gold nanostructures using photoemission electron microscopy [44], etc.

5. Conclusions

The GN has been of the significant importance due to their use for surface-enhanced Raman scattering. We analyzed four groups (with the sizes of 13, 17, 32, and 64 nm) of GN of different sizes at 400 and 800 nm using the 60 fs pulses propagating through the GN suspensions. The plasmonic resonance of GNs is far from 800 nm. We determined the optical, structural, and nonlinear optical characteristics of the GN suspensions synthesized by chemical method. Their nonlinear refractive indices, nonlinear absorption coefficients, and saturated intensities were measured. We studied the optical limiting of 800 nm, 60 fs pulses in 17 nm GN suspension and showed approximately four-fold limitation of propagated pulses with regard to the pure water. The competition of saturable and reverse saturable absorption in the case of 800nm pulses were analyzed at different energies of laser pulses.

As it was shown in present study, the nanorods, nanocubes, and nanoparticles of the same metal show completely different properties. That is the reason why many groups are working to develop different methods of synthesis of the metallic nanoparticles and particularly GN. Our work was aimed in the search of size-dependent nonlinear optical properties of GN at 400 nm (i.e. near the plasmonic resonance) and 800 nm (i.e. out of the plasmonic resonance). Our calculation of the β in the case of RSA (7×10^{-6} cm W^{-1}) in GN is among the largest reported so far for the metal nanoparticles. The intensity-dependent transformation from saturable absorption to reverse saturable absorption and excellent optical response indicate that the small-sized GN can be considered as potential candidate in passive mode locking and eye/device protection against powerful lasers.

Funding

Natural Science Foundation of China (NSFC) (61774155, 61705227); National Key Research and Development Program of China (2017YFB1104700); Chinese Academy of Sciences President's International Fellowship Initiative (Grant No. 2018VSA0001).

References

1. S. Guo and E. Wang, "Synthesis and electrochemical applications of gold nanoparticles," Anal. Chim. Acta **598**(2), 181–192 (2007).
2. W. R. Algar, M. Massey, and U. J. Krull, "The application of quantum dots, gold nanoparticles and molecular swtches to optical nucleic-acid diagnostics," Trends Analyt. Chem. **28**(3), 292–306 (2009).
3. K.-T. Yong, M. T. Swihart, H. Ding, and P. N. Prasad, "preparation of gold nanoparticles and their applications in anisotropic nanoparticle synthesis and bioimaging," Plasmonics **4**(2), 79–93 (2009).
4. D. Pissuwan, C. H. Cortie, S. M. Valenzuela, and M. B. Cortie, "Functionalised gold nanoparticles for controlling pathogenic bacteria," Trends Biotechnol. **28**(4), 207–213 (2010).
5. E. C. Dreaden, A. M. Alkilany, X. Huang, C. J. Murphy, and M. A. El-Sayed, "The golden age: gold nanoparticles for biomedicine," Chem. Soc. Rev. **41**(7), 2740–2779 (2012).
6. H. Jans and Q. Huo, "Gold nanoparticle-enabled biological and chemical detection and analysis," Chem. Soc. Rev. **41**(7), 2849–2866 (2012).
7. S. C. Mehendale, S. R. Mishra, K. S. Bindra, M. Laghate, T. S. Dhami, and K. S. Rustagi, "Nonliear refraction in aqueous colloidal gold," Opt. Commun. **133**(1–6), 273–276 (1997).

Optical Materials EXPRESS

8. R. A. Ganeev and T. Usmanov, "Nonlinear optical properties of various media," Quantum Electron. **37**(7), 605–622 (2007).
9. D. Wu, J. Peng, Z. Cai, J. Weng, Z. Luo, N. Chen, and H. Xu, "Gold nanoparticles as a saturable absorber for visible 635 nm Q-switched pulse generation," Opt. Express **23**(18), 24071–24076 (2015).
10. L. W. Tutt and A. Kost, "Optical limiting performance of C_{60} and C_{70} solutions," Nature **356**(6366), 225–226 (1992).
11. N. Venkatram, D. N. Rao, and M. A. Akundi, "Nonlinear absorption, scattering and optical limiting studies of CdS nanoparticles," Opt. Express **13**(3), 867–872 (2005).
12. W. Ji, H. J. Du, S. H. Tang, and S. Shi, "Nanosecond reverse satureable absorption in cubanelike transition-metal clusters," J. Opt. Soc. Am. B **12**(5), 876–881 (1995).
13. R. A. Ganeev, A. I. Ryasnyansky, M. K. Kodirov, S. R. Kamalov, and T. Usmanov, "Nonlinear susceptibilities, absorption coefficients and refractive indices of colloidal metals," J. Phys. D Appl. Phys. **34**(11), 1602–1611 (2001).
14. R. A. Ganeev, A. I. Ryasnyansky, M. K. Kodirov, and T. Usmanov, "Nonlinear optical characteristics of C60 and C70 films and solutions," Opt. Commun. **185**(4–6), 473–478 (2000).
15. M. Sheik-Bahae, A. A. Said, and E. W. Van Stryland, "High-sensitivity, single-beam n_2 measurements," Opt. Lett. **14**(17), 955–957 (1989).
16. L. W. Tutt and T. Boggess, Prog. "A review of optical limiting mechanisms and devices using organics, fullerenes, semiconductors and other materials," Quantum Electron. **17**(4), 299–338 (1993).
17. G. Ramakrishna, O. Varnavski, J. Kim, D. Lee, and T. Goodson, "Quantum-sized gold clusters as efficient two-photon absorbers," J. Am. Chem. Soc. **130**(15), 5032–5033 (2008).
18. Y. Yang, M. Nogami, J. Shi, H. Chen, G. Ma, and S. Tang, "Controlled surface-plasmon coupling in SiO_2-coated gold nanochains for tunable nonlinear optical properties," Appl. Phys. Lett. **8**(8), 081110 (2006).
19. I. Mirza, D. McCloskey, W. J. Blau, and J. G. Lunney, "Mechanism of large optical nonlinearity in gold nanoparticle films," Opt. Lett. **43**(7), 1455–1458 (2018).
20. L. D. Boni, E. L. Wood, C. Toro, and F. E. Hernandez, "Optical saturable absorption in gold nanoparticles," Plasmonics **3**(4), 171–176 (2008).
21. H. I. Elim, J. Yang, J. Y. Lee, J. Mi, and W. Ji, "Observation of saturable and reverse-saturable absorption at longitudinal surface plasmin resonance in gold nanorods," Appl. Phys. Lett. **88**(8), 083107 (2006).
22. K. S. Lee and M. A. El-Sayed, "Dependence of the enhanced optical scattering efficiency relative to that of absorption for gold metal nanorods on aspect ratio, size, end-cap shape, and medium refractive index," J. Phys. Chem. B **109**(43), 20331–20338 (2005).
23. X. Liu, X. Jia, M. Fischer, Z. Huang, and D. R. Smith, "Enhanced two-photon photochromism in metasurface perfect absorbers," Nano Lett. **18**(10), 6181–6187 (2018).
24. J. T. Seo, Q. Yang, W. J. Kim, J. Heo, S. M. Ma, J. Austin, W. S. Yun, S. S. Jung, S. W. Han, B. Tabibi, and D. Temple, "Optical nonlinearities of Au nanoparticles and Au/Ag coreshells," Opt. Lett. **34**(3), 307–309 (2009).
25. X. Ji, X. Song, J. Li, Y. Bai, W. Yang, and X. Peng, "Size control of gold nanocrystals in citrate reduction: the third role of citrate," J. Am. Chem. Soc. **129**(45), 13939–13948 (2007).
26. K. Dota, J. A. Dharmadhikari, D. Mathur, and A. K. Dharmadhikari, "Third-order nonlinear optical response in transparent solids using ultrashort laser pulses," Appl. Phys. B **107**(3), 703–709 (2012).
27. D. Blömer, A. Szameit, F. Dreisow, T. Schreiber, S. Nolte, and A. Tünnermann, "Nonlinear refractive index of fs-laser-written waveguides in fused silica," Opt. Express **14**(6), 2151–2157 (2006).
28. P. N. Njoki, I. I. S. Lim, D. Mott, H.-Y. Park, B. Khan, S. Mishra, R. Sujakumar, J. Luo, and C.-J. Zhong, "Size correlation of optical and spectroscopic properties for gold nanoparticles," J. Phys. Chem. C **111**(40), 14664–14669 (2007).
29. M. A. Villegas, M. A. Garcia, J. Llopis, and J. M. Fernandez Navarro, "Optical spectroscopy of hybrid sol-gel coatings doped with noble metals," J. Sol-Gel Sci. Technol. **11**(3), 251–265 (1998).
30. X. Ji, X. Song, J. Li, Y. Bai, W. Yang, and X. Peng, "Size control of gold nanocrystals in citrate reduction: the third role of citrate," J. Am. Chem. Soc. **129**(45), 13939–13948 (2007).
31. K. Wang, H. Long, M. Fu, G. Yang, and P.-X. Lu, "Off-resonant third-order optical ninlinearity of Au nanoparticle array by femtosecond Z-scan measurement," Chin. Phys. Lett. **27**(12), 124204 (2010).
32. L. W. Tutt and T. F. Boggess, "A review of optical limiting mechanisms and devices using organics, fullerenes, semiconductors and other materials," Prog. Quantum Electron. **17**(4), 299–338 (1993).
33. R. A. Ganeev, G. S. Boltaev, R. I. Tugushev, T. Usmanov, and H. Kuroda, "Nonlinear optical absorption and refraction in Ru, Pd, and Au nanoparticle suspensions," Appl. Phys. B **100**(3), 571–576 (2010).
34. C. Zheng, J. Huang, L. Lei, W. Chen, H. Wang, and W. Li, "Nanosecond nonlinear optical and optical limiting properties of hollow gold nanocages," Appl. Phys. B **124**(1), 17 (2018).
35. R. Karimzadeh, H. Aleali, and N. Mansour, "Thermal nonlinear refraction properties of Ag2S semiconductor nanocrystals with its application as a low power optical limiter," Opt. Commun. **284**(9), 2370–2375 (2011).
36. L. Sarkhosh and N. Mansour, "Study of the solution thermal conductivity effect on nonlinear refraction of colloidal gold nanoparticles," Laser Phys. **25**(6), 065404 (2015).
37. S. J. Sheldon, L. V. Knight, and J. M. Thorne, "Laser-induced thermal lens effect: a new theoretical model," Appl. Opt. **21**(9), 1663–1669 (1982).

Optical Materials EXPRESS

38. X. L. Zhang, Z. B. Liu, X. C. Li, Q. Ma, X. D. Chen, J. G. Tian, Y. F. Xu, and Y. S. Chen, "Transient thermal effect, nonlinear refraction and nonlinear absorption properties of graphene oxide sheets in dispersion," Opt. Express **21**(6), 7511–7520 (2013).
39. M. Sheik-Bahae, A. A. Said, T.-H. Wei, D. J. Hagan, and E. W. Van Stryland, "Sensitive measurement of optical nonlinearities using a single beam," IEEE J. Quantum Electron. **26**(4), 760–769 (1990).
40. T. Ghambari and D. Dorranian, "Measurement of third-order nonlinear susceptibility of Au nanoparticles doped PVA film," Opt. Spectrosc. **119**(5), 838–848 (2015).
41. G. Jagannath, B. Eraiah, K. Naga Krishnakanth, and S. Venugopal Rao, "Linear and nonlinear optical properties of gold nanoparticles doped borate glasses," J. Non-Cryst. Solids **482**, 160–169 (2018).
42. M. Gu, H. Bao, X. Gan, N. Stokes, and J. Wu, "Tweezing and manipulating micro- and nanoparticles by optical nonlinear endoscopy," Light Sci. Appl. **3**(1), e126 (2014).
43. G. Hergert, J. Vogelsang, F. Schwarz, D. Wang, H. Kollmann, P. Groß, C. Lienau, E. Runge, and P. Schaaf, "Long-lived electron emission reveals localized plasmon modes in disordered nanosponge antennas," Light Sci. Appl. **6**(10), e17075 (2017).
44. Q. Sun, K. Ueno, H. Yu, A. Kubo, Y. Matsuo, and H. Misawa, "Direct imaging of the near field and dynamics of surface plasmon resonance on gold nanostructures using photoemission electron microscopy," Light Sci. Appl. **2**(12), e118 (2013).